PERSPECTIVES

Revision of the Starling principle: new views of tissue fluid balance

J R Levick
Physiology, St George's Hospital Medical School, London SW17 0RE, UK

Email: tvttfyheot63@hotmail.com

Tissue fluid balance, plasma volume regulation and clinical oedema formation are governed by the Starling principle of microvascular fluid exchange. This states that transendothelial filtration is driven by capillary pressure (P_c) and interstitial protein osmotic pressure (π_i), while a counteracting absorptive force is exerted by plasma protein osmotic pressure (π_p) and interstitial pressure (P_i). Since P_c falls along a capillary, the plausible concept of filtration from arterial capillaries and sustained reabsorption into venous capillaries has become embedded in the literature. Most of us learned this as first year undergraduates and took it to be a well proven, somewhat fossilized truth. In recent years, however, this 'accepted' view has undergone substantial experimental and theoretical re-evaluation; see the Classical Perspective by Michel (2004) in this issue of *The Journal of Physiology*. In particular, a landmark study of the P_c–filtration relation by Michel & Phillips (1987) demonstrated that although absorption occurs transiently at $P_c < \pi_p$, absorption cannot be sustained, probably because π_i increases with time. A further problem was the 'low lymph flow paradox', namely that net capillary filtration rate calculated from tissue-averaged Starling forces (including π_i) is much greater than the tissue

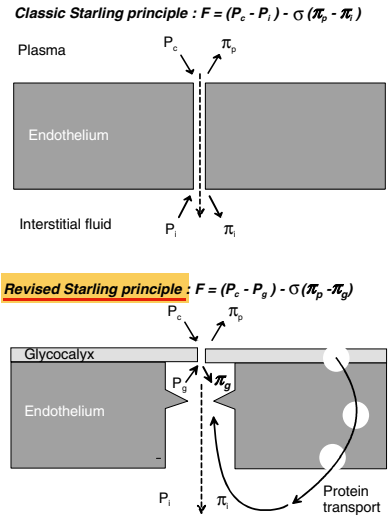

Figure 1. Changing nature of Starling principle for fluid exchange across non-fenestrated endothelium
F, sum of 'forces' acting across semipermeable membrane. σ, reflection coefficient. Other symbols as in text. Continuous short arrows denote force directions; dashed arrows denote flow.

lymph production. These observations, along with new structure–function findings, led to the proposal of novel endothelial filtration models by Michel and by Weinbaum (Michel, 2004 and below). Now Adamson *et al.* (2004), also in this issue of *The Journal of Physiology*, report a direct investigation of the little-studied effect of π_i on fluid exchange, with results that conflict dramatically with classical Starling predictions but support the Michel–Weinbaum model.

In an elegant, rigorous study, Adamson *et al.* (2004) measured trans-endothelial fluid flux in cannulated postcapillary venules (a non-fenestrated 'model' for capillaries) in the rat mesentery and changed π_i by albumin superfusion. The key finding was that raising π_i increased the filtration rate by only a small fraction of that predicted by the Starling principle. The fraction was 25% under their specific experimental conditions but depends on the filtration rate (see below). Continuous endothelium thus displays osmotic asymmetry, unlike the symmetrical Starling principle. Indeed, in an analogous study in frogs Professor Roy Curry's group found that altering π_i had virtually no effect at all on filtration rate (Hu *et al.* 2000).

Adamson *et al.* (2004) combined their experiments *in vivo* with confocal imaging of interstitial albumin distribution, reconstruction of the endothelial intercellular pathway geometry by serial electron micrography and a sophisticated mathematical model of the exchange pathway, to explain their results quantitatively. The semipermeable membrane (selective pores) across which protein osmotic pressure is exerted is the luminal glycocalyx of endothelium (Fig. 1). The outside of this membrane is not in direct contact with interstitial fluid (π_i) but is connected to it by a long, narrow but open paracellular cleft. The subglycocalyx fluid is of lower protein concentration than the interstitial fluid because it is dominated by a continuously formed ultrafiltrate (osmotic pressure π_g). Protein concentration is higher in the bulk interstitial fluid (30–60% of plasma concentration) because plasma proteins cross the endothelial barrier by a separate pathway, the large pore system. To have any effect on the glycocalyx, interstitial protein has to diffuse against the current of fluid sweeping out through the intercellular cleft.

Can the concept of osmotic asymmetry be generalized to other tissues? In the structurally different fenestrated capillary, the exit from the ultrafilter (glycocalyx overlying fenestral membrane apertures) is much less enclosed. Here an analogous but less extreme osmotic asymmetry has been observed; changes in π_i have 50% of the effect of changes in π_p. This is again due to an abluminal protein gradient, in this case around the filtering fenestrations (Levick, 1994). However, in the only other study of continuous (non-fenestrated) endothelium and π_i (Smaje *et al.* 1970) the results seem at first to conflict with the asymmetry model. Smaje *et al.* varied π_i around rat cremaster and rabbit omental capillaries perfused with blood at normal pressures and found that filtration rate increased linearly with π_i, in approximately the amount expected from the capillary filtration coefficient. Adamson *et al.* (2004) argue that this may be because native P_c and filtration velocity are low, allowing interstitial protein to diffuse up the cleft into the subglycocalyx space. (Control filtration rate was deliberately set high in the *Adamson et al.* study to test the concept of a 'protected' subglycocalyx space.) The authors estimate that 70–90% of the bulk π_i may be effective in the subglycocalyx space (π_g) under conditions of low P_c at heart level.

The new paradigm has important implications for fluid balance and oedema formation. First, it renders untenable the popular argument that sustained venular absorption accounts largely for tissue fluid balance. During fluid absorption the subglycocalyx π_g will increase quickly, due to reverse ultrafiltration, and thus prevent sustained absorption – as Michel & Phillips (1987) proved experimentally. To explain tissue fluid balance we must now focus increasingly on lymphatic function.

Second, the findings may help to resolve the low lymph flow paradox (see earlier). Use of bulk π_i overestimates the net filtration force and hence the lymph production, because the effective abluminal osmotic pressure π_g is smaller than π_i. The size of the difference is itself a function of filtration rate.

Third, reduction of bulk π_i is traditionally considered a major part of the 'safety margin' against oedema formation. This is evidently untrue at high filtration rates. Physiological filtration rates in many tissues, however, are probably slower than in the Adamson *et al.* experiment, so it remains possible that increases in filtration from low initial rates are buffered by reduced π_g. Indeed the authors argue that the effectiveness of this buffering process is enhanced. This could be tested by repeating their study over a range of π_i and P_c values.

The paper by Adamson *et al.* (2004) is an important step forward but it also raises a new, medically important puzzle; how is the life-supporting reabsorption of interstitial fluid sustained in clinical shock? In human hypovolaemic shock ~500 ml of interstitial fluid can be absorbed over ~30 min, topping up the depleted circulation, as Starling himself noted. Hyperglycaemic hyperosmolarity may influence the fluid shift in the whole animal. However, even in an isolated perfused cat or dog hind-limb, the absorption process can continue for 15 min. The steady-state model of Adamson *et al.* (2004) does not address the time course of reabsorption; but since the intercellular cleft volume is extremely small, a very short time constant might be implied, possibly seconds. The time course of absorption remains inadequately understood and constitutes a medically important challenge for the future.

Adamson RH *et al.* (2004). *J Physiol* **557**, 889–907.
Hu *et al.* (2000). *Am J Physiol* **279**, H1724–H1736.
Levick JR (1994). *Microvasc Res* **47**, 90–125.
Michel CC (2004). (Classical Perspective) *J Physiol* **000**, 000–000.
Michel CC & Phillips ME (1987). *J Physiol* **388**, 421–435.
Smaje LH *et al.* (1970). *Microvasc Res* **2**, 96–110.

DOI: 10.1113/jphysiol.2004.066118

Cardiovascular Research (2010) **87**, 198–210
doi:10.1093/cvr/cvq062

SPOTLIGHT REVIEW

Microvascular fluid exchange and the revised Starling principle

J. Rodney Levick[1] and C. Charles Michel[2]*

[1]Physiology, Basic Medical Sciences, St George's Hospital Medical School, London SW17 0RE, UK; and [2]Department of Bioengineering, Imperial College, Exhibition Road, London SW7 2AZ, UK

Received 30 November 2009; revised 4 February 2010; accepted 18 February 2010; online publish-ahead-of-print 3 March 2010

Microvascular fluid exchange (flow J_v) underlies plasma/interstitial fluid (ISF) balance and oedematous swelling. The traditional form of Starling's principle has to be modified in light of insights into the role of ISF pressures and the recognition of the glycocalyx as the semi-permeable layer of endothelium. Sum-of-forces evidence and direct observations show that microvascular absorption is transient in most tissues; slight filtration prevails in the steady state, even in venules. This is due in part to the inverse relation between filtration rate and ISF plasma protein concentration; ISF colloid osmotic pressure (COP) rises as J_v falls. In some specialized regions (e.g. kidney, intestinal mucosa), fluid absorption is sustained by local epithelial secretions, which flush interstitial plasma proteins into the lymphatic system. The low rate of filtration and lymph formation in most tissues can be explained by standing plasma protein gradients within the intercellular cleft of continuous capillaries (glycocalyx model) and around fenestrations. Narrow breaks in the junctional strands of the cleft create high local outward fluid velocities, which cause a disequilibrium between the subglycocalyx space COP and ISF COP. Recent experiments confirm that the effect of ISF COP on J_v is much less than predicted by the conventional Starling principle, in agreement with modern models. Using a two-pore system model, we also explore how relatively small increases in large pore numbers dramatically increase J_v during acute inflammation.

Keywords Starling principle • Glycocalyx • Fluid exchange

This article is part of the Spotlight Issue on: Microvascular Permeability

1. Introduction

The plasma, interstitial fluid (ISF), and lymph compartments are linked in series and, in the steady state, fluid flows continuously from one compartment to the next. Lymph drains back into the circulation chiefly at the major veins at the base of the neck. Accidental lymphatic fistulae in the neck indicate a total post-nodal lymph flow of up to 4 L/day in humans. Later work revealed that roughly half the fluid content of afferent lymph can be absorbed by lymph node microvessels,[1,2] raising the fluid turnover estimate to ~8 L/day.[3] This is a considerable fluid turnover; since human plasma volume is only ~3 L, the entire plasma volume (except the proteins) leaves the circulation approximately once every 9 h.

Substantial fluid movements between the plasma and interstitium account for the rapid swelling of acutely inflamed tissues (minutes), and for the oedematous swelling of venous thrombosis, cardiac failure, and lymphatic failure over hours to days. Conversely, haemodilution following an acute haemorrhage reveals a rapid absorption of ISF into the blood stream (~0.5 L in 15–30 min). Acute fluid transfers are important medically, because plasma volume is a major determinant of the cardiac filling pressure and thus cardiac output (Starling's 'law of the heart').

The fundamental principle governing such fluid shifts was laid down by Starling[4] in 1896. Starling[4] showed that isotonic saline injected into the interstitial compartment of a dog hind limb appeared in the venous blood, which became haemodiluted; but when serum rather than saline was injected, the fluid was not absorbed. Starling therefore proposed that the walls of capillaries (and post-capillary venules) are semipermeable membranes. Consequently, fluid movement across them depends on the net imbalance between the osmotic absorption pressure of the plasma proteins [colloid osmotic pressure (COP)] and the capillary hydraulic pressure generated by the heart beat. Starling also recognized that since ISF has a substantial concentration of plasma proteins, microvascular semipermeability is imperfect; the endothelial barrier slowly 'leaks' plasma proteins into the interstitium. The degree of leakiness to a specific solute can be quantified by Staverman's osmotic reflection coefficient,[5] σ, which ranges in value from 0 to 1; unity means perfect, 100% reflection, and thus no leakage of the specified solute. For a simple membrane separating well-stirred solutions of a single solute at two different

* Corresponding author. Tel: +44 14818823452, Email: c.c.michel@imperial.ac.uk

concentrations, it follows from the principles of irreversible thermodynamics[5,6] that:

$$\frac{J_v}{A} = L_p\{\Delta P - \sigma\Delta\Pi\}, \quad (1a)$$

where J_v is the volume filtration rate per unit endothelial area A, ΔP the difference in hydrostatic pressure, and $\Delta\Pi$ the difference in osmotic pressure across the membrane.

Plasma and ISF each contain many solutes (species 'n'). Therefore, to describe fluid movement across the intervening capillary wall, Eq. (1a) should be written as:

$$\frac{J_v}{A} = L_p\{\Delta P - \sum \sigma_n \Delta\Pi_n\}, \quad (1b)$$

where $\sum\sigma_n\Delta\Pi_n$ represents the sum of the differences in osmotic pressure exerted across the vessel walls by all the solutes in plasma and ISF. In Eq. (1b), ΔP is the difference between local capillary blood pressure P_c (diminishing with axial distance) and ISF hydrostatic pressure P_i. In most microvascular beds, only the macromolecular solutes are present at significantly different concentrations, and for the small solutes, σ has a value of 0.1 or less. Under these conditions, J_v can be described approximately by Eq. (1a), where $\sigma\Delta\Pi$ is the difference between the effective osmotic pressure exerted by the macromolecules (COP) in plasma (Π_p) and ISF (Π_i) (*Figure 1A*). This leads to the conventional expression

$$\frac{J_v}{A} = L_p\{(P_c - P_i) - \sigma(\Pi_p - \Pi_i)\}. \quad (1c)$$

If σ has a value close to 1.0 and both P_i and Π_i are close to zero, as in the following experimental studies, Eq. (1c) summarizes the classic observations of Landis[7] and Pappenheimer and Soto-Rivera,[8] whose investigations are generally regarded as having established Starling's hypothesis. By measuring the prevailing P_c by direct micropuncture in single capillaries in the frog mesentery and estimating the corresponding rates of filtration and absorption by a red cell tracking

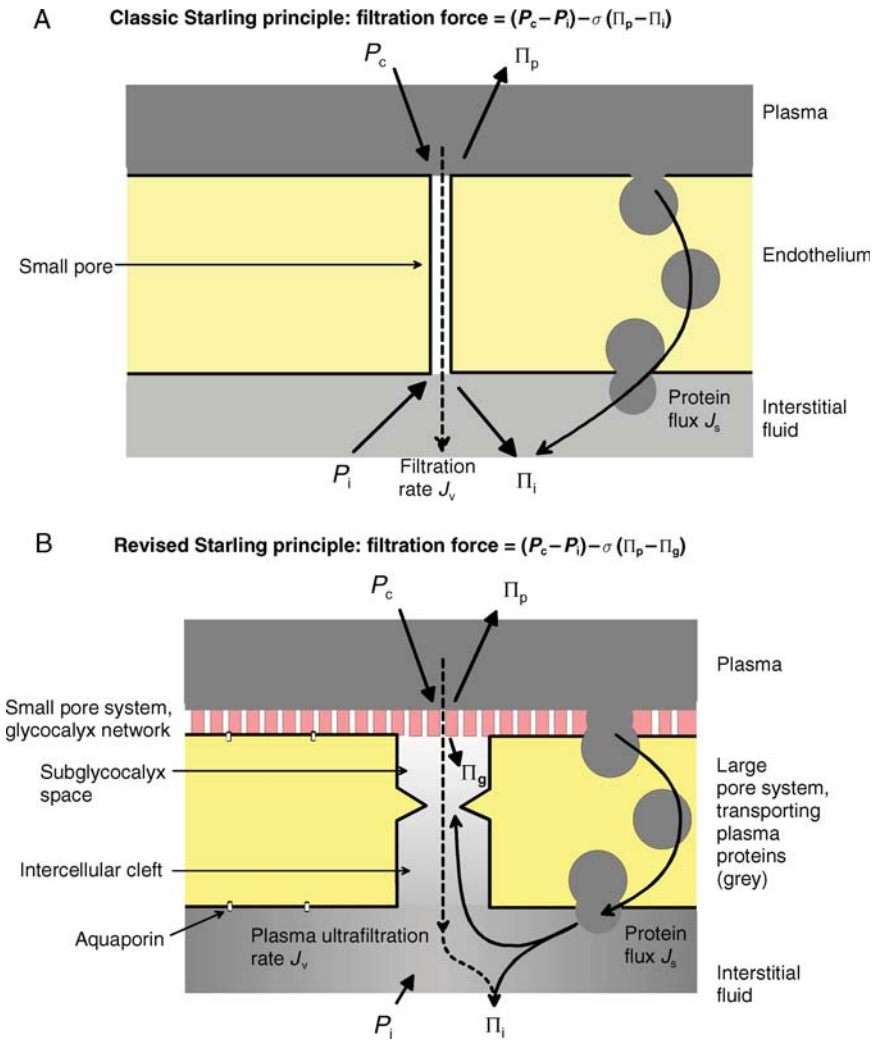

Figure 1 Comparison of traditional and revised views of the endothelial semipermeable membrane and the forces acting on it. (*A*) Traditional view of continuous endothelium as a semipermeable membrane. (*B*) The glycocalyx–cleft model identifies glycocalyx as a semipermeable layer. Its underside is subjected to the COP of fluid high inside the intercellular cleft rather than ISF, with important functional consequences.[80,82] Symbols defined in main text. Grey shade denotes concentration of plasma protein.

method, Landis was able to demonstrate a linear relation between J_v and P_c for a population of vessels. Using isolated perfused cat and dog hind limbs, Pappenheimer and Soto-Rivera ingeniously estimated the mean tissue P_c from the arterial and venous pressures and vascular resistances. They were able to vary mean P_c and demonstrated a linear correlation with rates of microvascular fluid filtration/absorption, estimated from changes in limb weight. Landis[9] also showed, using micropipettes inserted into human nailfold skin capillaries at heart level, that blood pressure falls along a capillary, from >45–35 mmHg at the arterial end to ≥12–15 mmHg at the venular end (depending on skin temperature[10,11]). This gave credence to a simple picture of fluid exchange symmetry first suggested by Starling.[12] The picture is that since P_c exceeds Π_p (25–28 mmHg in humans) over the arterial half of the capillary bed at heart level, there is fluid filtration here; and this is balanced by absorption over the venous half, where P_c falls below Π_p. The concept was developed by Landis and Pappenheimer[13] and although they circumspectly noted that '*with equal or greater licence* (our italics) an average limb capillary and lymphatic can be drawn', the caveat was largely ignored and the model became widely reproduced as an established fact (*Figure 2A*, left panel). It was not, however, based on a single tissue or species, because modern methods for measuring the important interstitial terms P_i and Π_i in human skin were not then available.[14] Over the past 25 years, it has become clear that the conventional model does not describe fluid exchange in the real microcirculation, because (i) both P_i and Π_i change when J_v changes, and (ii) the fluid immediately downstream of the semipermeable membrane (the subglycocalyx fluid, see later) can have a markedly different composition to bulk ISF.

In this short review, we first consider data bearing on the conventional steady-state filtration–reabsorption model, then experiments highlighting the distinction between the linear, transient fluid exchange

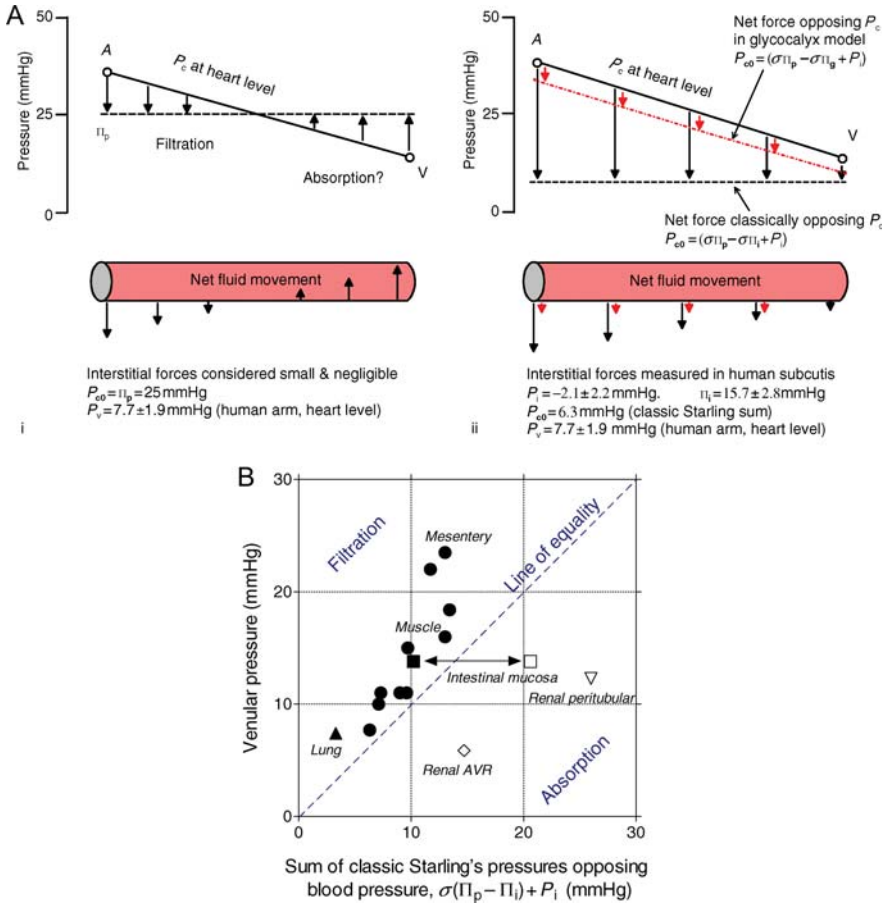

Figure 2 Imbalance of the classical Starling pressures when all four terms are measured in the same tissue and species. (*A*) *Left panel* shows the traditional filtration–reabsorption model; interstitial terms are considered negligible. *Right panel* shows the imbalance when all four classic Starling forces are measured in human skin and subcutis at heart level.[18] Black arrows indicate net force imbalance and hence the direction and the magnitude of fluid exchange are based on the four classic forces. Dot-dashed line (red) illustrates qualitatively the much smaller net filtration force predicted by the glycocalyx–cleft model. For symbols see text. (*B*) Sum of three classic Starling forces opposing microvascular blood pressure ($P_{c0} = \sigma\Pi_p - \sigma\Pi_i + P_i$) plotted against the lowest microvascular blood pressure in different tissues (P_c). Each point is based on measurements in the same tissue and species except the intestine (square symbols), where P_c value from rats are plotted against values P_{c0} derived from cats. Closed square is non-absorbing intestine; open square is during water absorption from gut lumen. P_{c0} is capillary pressure at which the classic net filtration force would be zero. If venular pressure exceeds P_{c0} (i.e. lies above the line of equality), venules and venous capillaries are in a state of filtration. Data from many laboratories.[19]

vs. pressure relation and the non-linear, steady-state relation. This is followed by a review of the altered perspective resulting from the recognition of the glycocalyx as the semipermeable layer coating the inside of the capillary wall. For a broad overview of endothelial physiology, see Levick.[15]

2. Traditional filtration–reabsorption model vs. Starling pressures measured in specific tissues: sum-of-forces evidence

Doubts about the validity of the filtration–absorption model surfaced quietly at first. In a study of rabbit mesenteric and omental capillaries, using the Landis red cell method to monitor fluid exchange, Zweifach and Intaglietta[16] noted briefly 'We have not to date . . . encountered vessels that consistently showed inward filtration' (i.e. absorption). Ten years later, Levick and Michel[10] documented how human skin capillary pressure increases with distance below heart level, albeit partially protected by postural vasoconstriction of the pre-capillary resistance vessels; and they pointed out that tissue fluid balance cannot be maintained by downstream reabsorption in skin more than ~10 cm below heart level, because venous capillary P_c then exceeds Π_p.[10,17] In skin capillaries above the heart, P_c does not decrease in an analogous way, because the superficial veins collapse and P_c becomes independent of further elevation.[9] The issue of downstream force balance in human skin at heart level was addressed by Bates *et al.*,[18] who measured the interstitial terms using acutely inserted wicks. This enabled the sum of all four Starling pressures to be calculated. They found that due to the subatmospheric nature of P_i (−2 mmHg) and the substantial magnitude of Π_i (15.7 mmHg), there was no net absorptive force in the cutaneous venous capillaries or venules at heart level ($\Delta P > \sigma\Delta\Pi$) (*Figure 2A*, right panel). A review of the literature revealed the same situation in 14 different tissues/species, including skeletal muscle (~40% of body mass) and the lung, the tissue with the lowest P_c (*Figure 2B*). It is important to note that since the Starling pressures differ between tissues and species, a correct sum of forces necessitates measurement of all four forces in the same tissue.[19] The absence of a net absorptive force in downstream vessels in the steady state is in line with theoretical expectations, since a large $\Delta\Pi$ only develops in tissues with large filtration rates (see later). On the basis of today's glycocalyx–cleft model, Π_i is not the correct term to use in sum-of-force calculations (it should be the COP beneath the glycocalyx, Π_g, see below). However, the inference, i.e. no downstream net absorptive force in the steady state, remains valid, because absorption would raise extravascular Π and thus reinforce the sum-of-forces argument.

3. Absorption is observed transiently but not in the steady state at capillary pressures below plasma COP

The traditional steady-state filtration–reabsorption model was tested directly by Michel and Phillips.[20] They used a development of the Landis red cell method to measure the direction and rate of fluid exchange in perfused single capillaries of the frog mesentery under two different conditions. In one set of experiments, P_c was raised or lowered abruptly and fluid exchange was measured immediately after the change; no time was allowed for the extravascular forces to change (transient state). In a second set of experiments, P_c was maintained constant for at least 2 min (and usually longer) before measuring the filtration or absorption rate at the same value of P_c (steady state). As in Landis's study,[7] there was a linear relation between J_v/A and P_c in the transient experiments, with transient fluid absorption when P_c was lowered below $\sigma\Pi_p$. In the steady state, however, a dramatically different relation emerged (*Figure 3A*). When P_c exceeded $\sigma\Pi_p$, filtration rate again increased linearly with P_c; but when P_c was lower than $\sigma\Pi_p$, no absorption occurred in the steady state—contrary to the traditional downstream reabsorption model or transient state. The observations have been confirmed in both frog and rat mesenteric vessels[21] and analogous results were obtained in a study of filtration/absorption across confluent cultured endothelium in an Ussing-style chamber.[22]

Thus, capillaries with a low blood pressure can absorb fluid transiently but not in the steady state (the lungs are an important example)—in keeping with the sum-of-forces evidence presented earlier. Why is this so generally the case? The reason is that an additional principle influences the steady state besides the Starling principle, namely the coupling of extravascular plasma protein concentration (and hence Π_i) to capillary filtration rate. Furthermore, in some tissues, such as the lung and subcutaneous tissue, P_i increases non-linearly with ISF volume following increases in J_v/A.[14]

4. Inverse dependence of pericapillary COP on filtration rate restricts absorption to transient state in most tissues

As reviewed by Taylor and Granger,[23] in the steady state, the concentration of ISF plasma protein, C_i (determining Π_i), is not a fixed quantity but is inversely related to the capillary filtration rate; see the extravascular dilution curve of *Figure 3B*, right panel.[24] This is because ISF is continually renewed and C_i is determined dynamically by the rate of solute influx, J_s, relative to the rate of water influx J_v.

$$C_i = \frac{J_s}{J_v}. \quad (2)$$

It has been known for over 120 years (see Cohnheim[25]) that raising the capillary filtration rate 'dilutes' the macromolecules of the ISF and lymph.[3,26] Here, we encounter a tricky situation; J_v depends partly on extracapillary protein concentration[4] [Eq. (1a–c)]; but extracapillary protein concentration depends partly on J_v [the extravascular dilution curve, Eq. (2)]. By dividing the standard convection–diffusion equation for macromolecular transport (J_s) by J_v, Michel[27] derived an expression for C_i and hence Π_i in terms of J_v. This was then substituted into Eq. (1c) to predict the steady-state relation between J_v and P_c. The resulting, somewhat complex, expression [Eq. (3)] describes a curve that fits data for fluid exchange in the lung[28] and human limbs[29] and conforms closely to the steady-state results of Michel and Phillips,[20] with no sustained

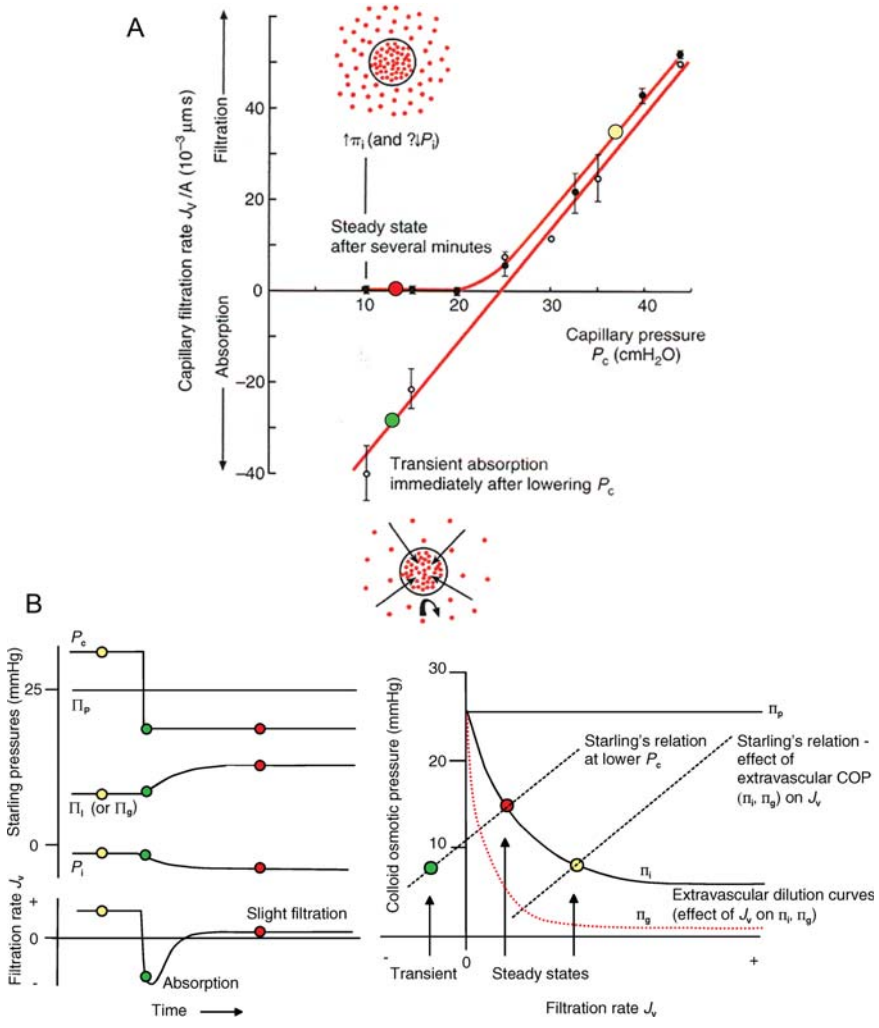

Figure 3 Direct observation of direction of fluid exchange in capillaries in which P_c is maintained below Π_p. (*A*) Comparison of fluid exchange immediately after raising or lowering P_c (transient state) and after P_c has been held constant for several minutes (steady state). Measurements made on single frog mesenteric capillaries perfused *in situ* with a Ringer solution plus serum albumin and the macromolecule Ficoll 70 ($\Pi_p = 32$ cmH_2O). When P_c was lowered from 30 to 10–15 cmH_2O, a brisk uptake of fluid into the capillary was observed (e.g. green point on transient relation). If the vessel was now perfused with P_c held constant in this range (10–15 cmH_2O), absorption attenuated and after several minutes could no longer be detected (red point on steady-state curve).[20] Insets illustrate concentration of pericapillary plasma protein (dots) following transient water absorption (long thin arrows) and interstitial plasma protein reflection (thick curved arrow). (*B*) Explanatory sketches. *Left panel* shows how extravascular Starling forces change with time (transient state) when P_c is lowered below Π_p, until a new steady state is reached. In intact tissues (cf. superfused mesentery), the absorption phase probably lowers P_i as well as raising pericapillary Π_p, further cancelling the net absorptive term. *Right panel* shows how the intersection of the Starling and extravascular dilution relations determines the steady state. The curvilinear ISF relation[23,24,100] describes the effect of filtration on ISF COP Π_i (red line indicates corresponding Π_g), while the linear, Starling's relation describes effect of extracapillary COP on filtration. Note that the latter relation is plotted contrary to convention, with the independent variable Π_i on the *y*-axis and dependent variable J_v on the *x*-axis.

reabsorption even at $P_c \ll \sigma\Pi_p$ (*Figure 3A*):

$$\frac{J_v}{A} = L_p\left[\Delta P - \sigma^2\Pi_p\frac{(1-e^{-Pe})}{(1-\sigma.e^{-Pe})}\right], \qquad (3)$$

where $Pe = J_v(1-\sigma)/p_dA$ and p_d is the diffusional permeability of the capillary barrier to the macromolecule. *Pe*, the Péclet number, is the ratio of the velocity at which the macromolecule is washed through by convection (solvent drag) to its diffusive velocity within the endothelial barrier.

It is important to note that Eq. (3) does not predict J_v/A in terms of ΔP, since J_v/A is present on the right-hand side too, hidden within the Péclet number. The equation can be rearranged to express ΔP as a function of J_v/A (see Appendix, end of this article) and this is how it is solved.[27]

The reason that Eq. (3) predicts no absorption of fluid at values of ΔP less than $\sigma\Delta\Pi$ is illustrated in *Figure 3B* (left panel). When P_c and J_v are reduced, C_i and Π_i rise with time [Eq. (2)]. This progressively reduces the absorptive force $\Pi_p - \Pi_i$, until the system finally reverts to slight filtration, at which point a new steady state is reached.

Rather than solving the Starling and extravascular dilution equations mathematically, one can draw out the linear, transient Starling's relation [J_v vs. Π_i for a given P_c, Eq. (1c)] and the interstitial dilution curve [C_i and hence Π_i vs. J_v, Eq. (2)] on the same graph, as in *Figure 3B*. The intersection point is the steady-state value. The intercept is always a positive J_v value, even as P_c approaches zero.[19]

In view of the coupling of Π_i to J_v, steady-state (but not transient) absorption in venous capillaries and venules is unlikely in most tissues. As Starling himself succinctly pointed out[4] 'With diminished capillary pressure there will be an osmotic absorption of salt solution from the extravascular fluid, until this becomes richer in proteids (*Figure 3B*, left panel); and the difference between its proteid osmotic pressure and that of the intravascular plasma is equal to the diminished capillary pressure'.

Perhaps, the most surprising finding of Michel and Phillips[20] was the speed with which a steady state of fluid exchange was established. In other tissues, the time constant is considerably longer, being of the order of tens of minutes for microvessels in the skeletal muscles of large mammals.[8] This may be because differences in the architecture of the pericapillary spaces allow protein concentration gradients to develop more rapidly in some tissues than others (see below). In addition, the time course may be influenced by aquaporins (water-only conducting pores in the endothelial cell membranes), which may contribute significantly to L_p in skeletal muscle microvessels[30–32] (see later).

5. Exceptions to the 'no steady-state absorption' rule: effect of local epithelial transport

There are physiologically important exceptions to the 'no steady-state absorption' rule. In the kidney, fluid is continuously taken up by the peritubular capillaries of the cortex and by the ascending vasa recta (AVR) of the medulla. In the intestine during water absorption, fluid is absorbed continuously by the mucosal capillaries. In lymph nodes, the capillaries continuously take up fluid from the inflowing pre-nodal lymph (see earlier). How do these vessels manage to break the rule? In lymph nodes, the ISF is continuously replaced by pre-nodal lymph of low protein concentration. In the kidney and the intestine, the ISF is renewed by an independent stream of protein-free fluid which is secreted by the neighbouring epithelia. The rapid renewal of the ISF breaks the inverse coupling between J_v and Π_i [Eq. (2)] and is often accompanied by a rise in P_i. When this explanation was first proposed,[27] it appeared to be consistent with data for the small intestine and renal cortex peritubular capillaries. In these tissues, the protein leaking into the ISF from the plasma is flushed into the local lymphatics by the epithelial secretions. For the renal AVR, however, the theory was less certain, because no lymphatic drainage from the medullary ISF has yet been demonstrated (see below). It should be noted that none of the microvessels in which steady-state absorption is maintained have the low continuous endothelium found in the skin, muscle, and connective tissue.

5.1 Intestinal mucosa

Although 70% of the blood flow to the rat ileum supplies the mucosa, direct microvascular pressure measurements showed that P_c in the fenestrated mucosal vessels lies well below P_c in the continuous capillaries of the parallel microcirculations of the circular and longitudinal smooth muscle.[33] In cats, the intestinal lymph flow increases and its protein concentration decreases as fluid is absorbed from the small intestine lumen.[34] In the non-absorbing ileum, lymph COP (Π_L) had a mean value of 10 mmHg, whereas during brisk fluid uptake, Π_L fell to 3 mmHg. The fall in Π_i must be as least as great, because intestinal fluid absorption increases the local ISF volume, which reduces the fractional exclusion of serum albumin.[35] The latter should amplify the reduction in Π_i. Assuming that (i) P_c is approximately the same in the absorbing and non-absorbing states and (ii) similar values for P_c are present in cat and rat mucosal capillaries, the Starling pressures across the capillary walls change from favouring a low level of filtration when the gut is not absorbing fluid to a state of sustained fluid uptake when the gut is absorbing fluid (*Figure 2B*).

During the absorption of digested food, this simple picture may be complicated by osmotic gradients set up by the absorbed small solutes. At high rates of glucose uptake, the glucose concentration difference across the walls of the capillaries at the tips of intestinal villi may rise to 70 mM. Even if the osmotic reflection to glucose at the walls of these vessels is as low as 0.01, the effective osmotic pressure set up by this glucose gradient opposes and exceeds the Starling pressures by 15 mmHg.[36] It is suggested that since the epithelial absorption of glucose and amino acids is confined to the outer third of the villus, fluid absorbed through epithelium here might flow through the villus interstitium to be taken up into the extensive capillary bed of the lower two-thirds of the villi[36] and into the lacteals.

5.2 Renal cortex

The peritubular capillary Starling forces have been determined in rat and dog kidneys by several workers and mean values are shown in *Table 1* for hydropenic rats and for rats with ISF volumes expanded by isotonic saline.[37] In hydropenic rats, the Starling pressures favour fluid uptake, due to relatively low values of P_c and Π_i and relatively high values of P_i and Π_p. Local Π_p is 20–30% higher than in systemic arterial blood, because the peritubular vessels are fed with plasma concentrated by glomerular filtration. Following ISF expansion by intravenous saline infusion, local Π_p is reduced and P_c is increased but the net pressure favouring fluid uptake is maintained by a large increase in P_i and a further fall in Π_i. Similar observations have been made in hydropenic and volume expanded dogs. The low concentration of interstitial plasma protein, and hence Π_i, is maintained by the low macromolecular permeability of the fenestrated peritubular capillaries ($\sigma_{albumin} \approx 0.99$) and the fast production of protein-free ISF by the tubular epithelium, which flushes the relatively small amount of plasma protein entering the cortical ISF into the cortical lymphatics.

5.3 Renal medulla

Fluid that is absorbed by the collecting ducts from the nascent urine is cleared continuously from the medullary ISF by absorption into the AVR. Estimates of the Starling pressures across the walls of the AVR in the inner medulla of rats indicate high values of Π_p and P_i and low values of P_c and Π_i, consistent with high rates of fluid uptake (*Table 1*).

Until recently, the low value of Π_i (implying good protein clearance) was puzzling for two reasons. Unlike the cortical peritubular capillaries, the AVR have a relatively high permeability to plasma protein; and unlike the cortex, lymphatic drainage has never been demonstrated convincingly in the renal medulla. In both dogs[38] and rats,[39] labelled plasma protein reached 85% of its steady-state

Table 1 Starling pressures (mmHg) across the walls of peritubular capillaries and AVR in rat kidney

Cortical peritubular capillaries ($\sigma_{albumin} = 0.99$)					
Fluid balance	Π_p	Π_i	P_c	P_i	$\sigma\Delta\Pi - \Delta P$
Hydropenia (mean ± SEM)	24.8 ± 1.39	3.9 ± 0.6	13.2 ± 1.3	3.3 ± 0.6	10.0
Volume expanded (mean ± SEM)	16.6 ± 1.34	1.3 ± 0.18	19.5 ± 2.71	11.5 ± 0.78	7.1
Ascending vasa recta of the renal medulla ($\sigma_{albumin} = 0.7$)					
Hydropenia	Π_p	Π_i	P_c	P_i	$\sigma\Delta\Pi - \Delta P$
Papilla tip (mean ± SEM)	26.0 ± 2.3	3.7 ± 0.26	7.8 ± 0.4	6.0 ± 0.3	13.8
Papilla base (mean ± SEM)	16.7 ± 1.3	3.7 ± 0.26	6.7 ± 0.48	6.0 ± 0.3	8.4

The column headed $\sigma\Delta\Pi - \Delta P$ lists values for the net Starling pressure favouring fluid absorption into the vessels. Data for cortical peritubular capillaries are based on four studies summarized by Ulfendahl and Wolgast.[37] Data for ascending vasa recta of the renal medulla are from several laboratories reviewed by MacPhee and Michel[43] and Michel.[45]

concentration in the renal medullary ISF within 3 min of its injection into the circulation. Ultrastructural studies have shown that ferritin, catalase, and horseradish peroxidase can pass through the fenestrae of the AVR into the ISF.[40] It was believed that pre-lymphatic channels might drain medullary ISF[41] into the renal cortex but these have not been confirmed. Relatively recently, Tenstad *et al.*[42] demonstrated that labelled albumin is cleared from the medullary ISF directly into the blood. To account for this, MacPhee and Michel[43] suggested that proteins might be washed into the AVR (convective protein transport) during fluid absorption, as follows.

If convective transport of protein from ISF into AVR is to be effective, the AVR σ to plasma proteins has to be significantly <1. Measurements of $\sigma_{albumin}$ in single perfused AVR have given values between 0.59 and 0.78.[43,44] With σ in this range, and protein-free fluid from the collecting ducts replacing the fluid passing into the AVR, calculations indicated that convective clearance into the AVR (driven by the Starling pressures, *Table 1*) can maintain a low ISF albumin concentration.[43,45] More detailed modelling[46,47] has provided additional support for the effectiveness of convective protein uptake in the medullary countercurrent exchange system.

Although P_c in the AVR is normally greater than the surrounding P_i, it is possible that P_i might exceed P_c if medullary ISF volume is rapidly increased. Because the hydraulic permeability of the fenestrated AVR is high ($\sim 100 \times 10^{-7}$ cm/s/cmH_2O), relatively large volumes of fluid carrying a low concentration of protein can be driven into the AVR by a trans-endothelial hydrostatic pressure difference of just 2–3 cmH_2O. Although a high P_i threatens to compress the AVR, these vessels were observed not to collapse until P_c fell more than 4 cmH_2O below atmospheric pressure.[48] The mechanical stability of the AVR is probably achieved by tethering of the endothelial cells to the basal lamina of neighbouring descending vasa recta and tubules by the fine processes described by Takahashi-Iwanaga.[49]

6. Low filtration force paradox

On the basis of the three lines of evidence reviewed above (sum of measured forces, direct observation of fluid exchange at low P_c, and theoretical considerations), tissue fluid balance in the muscle, skin, lung, and many other tissues is unlikely to be achieved through a near-balance of upstream filtration and downstream reabsorption in the steady state as traditionally supposed. The drainage of capillary filtrate by the lymphatic system is therefore the dominant factor responsible for interstitial volume homeostasis.[50] This view, however, introduces a new problem. As pointed out by Aukland and Reed,[51] the lymph flow predicted by Eq. (1a–c) from measurements of L_pA and the four classic Starling forces is often an order of magnitude bigger than the observed lymph flow. To express this paradox another way, the true, globally averaged net filtration force calculated from the rate of generation of lymph (~1 mmHg in many tissues) is much smaller than $(P_c - P_i) - \sigma(\Pi_p - \Pi_i)$, which is typically 5–10 mmHg (*Figure 2B*)—a discrepancy too large to dismiss as measurement error.

Several possible solutions have been proposed. In tissues with marked arteriolar vasomotion cycles (e.g. some skeletal muscles), the arteriolar contraction phase will lower P_c in the downstream capillary module,[8] leading to transient fluid absorption (*Figure 3*, transient line), followed by reversion to filtration during the arteriolar relaxation phase, as first suggested by Chambers and Zweifach[52] and developed by Intaglietta and Endrich.[53] In this model, fluid balance is temporal rather than spatial. Not all tissues, however, show the regular, strong vasomotion pattern on which the temporal model is based.

More recently, exciting new insights into the complex pore structure of endothelium have helped to resolve the low filtration force paradox, by showing that the true net filtration force across endothelium depends not so much on Π_i as on the COP of fluid just below the endothelial glycocalyx. In the next section, we will see that the plasma protein concentration here can be substantially less than that in the bulk ISF.

7. Pore exit microgradients and the glycocalyx–cleft model for continuous capillaries

7.1 Fenestrated capillaries

The classic Starling principle is symmetrical—the effect of increases in Π_i is predicted to have the same effects on fluid exchange as decreases in Π_p. This proved not to be the case, however, when tested in the fenestrated capillaries of synovium, the tissue that lines joint cavities. Synovial capillaries lie just a few micrometres below the highly porous surface of the tissue, with small clusters of fenestrae (1–2% of surface) orientated towards the joint cavity. Consequently, intra-articular infusions of albumin can be used to alter Π_i, while measuring the resulting change in trans-synovial flow.[54] When the response was compared with that brought about by changes in Π_p following intravascular albumin perfusion, a marked asymmetry was

observed. Changes in bulk Π_i had approximately one-third as much effect on fluid exchange as changes in Π_p. A two-dimensional model of synovial fluid exchange indicated that the explanation lay in the development of gradients of ISF albumin concentration (and hence Π_i) around the exits from the fenestral clusters, supported by the poorly stirred nature of ISF.[55] The ISF COP adjacent to the fenestrations was substantially lower than in the bulk ISF, because the ultrafiltrate emerging from the fenestrations diluted the immediately adjacent ISF over several micrometres. In other words, plasma ultrafiltration set up 'microgradients' of ISF protein concentration (steep gradients over micrometre distances). The generality of these findings has yet to be tested in other fenestrated capillary beds.

7.2 Continuous capillaries

7.2.1 Structure of intercellular pathway

Asymmetrical behaviour is even more extreme in continuous capillaries. Here, the principal fluid-conducting pathways are through the endothelial intercellular clefts. (In most microvessels, aquaporins in the endothelial cell membranes contribute $\leq$10% of the hydraulic conductance, except in blood–brain barrier and possibly skeletal muscle capillaries.[56] Aquaporins have a role when interstitial osmolarity increases, e.g. renal descending vasa recta[57] and swelling, 'pumped' exercised muscle.[30]) Ultrastructural studies show that the pathway through the intercellular cleft follows a long, narrow, tortuous route.[58–60] The cumulative perimeters of the cells over 1 cm^2 endothelium (i.e. total length of the luminal entrance to the intercellular clefts in the surface plane) is a remarkable 12–20 m. Within the clefts, however, 90% of this length is sealed by the junctional strands ('tight junctions'). Fluid is funnelled through breaks in the strands that occur at 2–4 μm intervals, each break being only 200–400 nm in length (*Figure 4A*). The clefts are 14–21 nm wide throughout; they do not narrow at the breaks in the junctional strands. Consequently, the breaks are too wide to filter out the plasma proteins (molecular diameter of serum albumin 7.1 nm). The protein-reflecting element or 'small pore' system has an effective diameter of ~8 nm.[23,61–63] Based partly on these considerations, Curry and Michel[64] proposed that the ultrafiltering pores are located in the 'fibre-matrix' of the endothelial luminal glycocalyx, which overlies the entrance to the clefts.

The glycocalyx is a complex, quasi-periodic network of glycosaminoglycan chains (syndecan-1, glypican, and hyaluronan) and sialoglycoproteins, extending 60–570 nm from the endothelial luminal membrane and coating the inner surface of capillaries, including the entrance to the intercellular cleft and most fenestrations.[65–68] Evidence that the glycocalyx is a major determinate of capillary permeability includes large increases in L_p when glycocalyx-binding proteins are removed from the capillary perfusate (the 'protein' effect[69–72]) or when glycocalyx components are removed by enzymatic digestion,[73,74] and direct observations.[75] Enzyme digestion studies also indicate that the glycocalyx mediates shear-induced changes in L_{pd}.[76] In addition to the glycocalyx–intercellular cleft pathway for water and small solutes, a separate, parallel 'large pore system' transports plasma proteins slowly into the interstitial compartment. This system comprises, controversially, large (≥50 nm wide) pores and/or vesicular transport.[77–79]

7.2.2 COP difference across the intercellular pathway

Michel[80] and Weinbaum[81] independently recognized that since the pathway for macromolecules for continuous endothelium lies in parallel with the main fluid-conducting pathway (intercellular clefts), the COP difference across the vascular barrier could no longer be calculated as Π_p minus Π_i. The COP difference that determines fluid exchange is that across the semipermeable glycocalyx. The fluid at the abluminal side of the glycocalyx is separated from the pericapillary ISF by the tortuous path through the intercellular clefts (*Figure 4A*) and since there can be protein concentration gradients along this path, Eq. (1c) should be written as:

$$\frac{J_v}{A} = L_p\{(P_c - P_i) - \sigma(\Pi_p - \Pi_g)\}, \quad (4)$$

where Π_g is the COP of the ultrafiltrate on the underside of the glycocalyx. Π_g can be very low, for two reasons; σ is high, and the outward flow of the ultrafiltrate prevents protein diffusion equilibrium between the subglycocalyx fluid and the pericapillary ISF. The diffusion disequilibrium is greatly exacerbated by cleft structure. As the ultrafiltrate converges to pass through the narrow breaks in the intercellular junctional strands, the fluid velocity increases at least 10-fold (*Figure 4A*), impeding the upstream diffusion of ISF plasma proteins.[60,80–82] Rough calculations indicate that even the low fluid filtration rate generated by a pressure difference of 1 cmH_2O suffices to prevent protein diffusion equilibrium between the subglycocalyx fluid and pericapillary ISF at the cleft exit.[80,81]

The above concept was developed into a two-dimensional mathematical model by Weinbaum and coworkers.[60,82] The model predicts intercellular cleft flow and plasma protein concentration in the subglycocalyx space for a given bulk ISF composition. Depending on the magnitude of the filtration pressure P_c, the model predicts big differences between subglycocalyx plasma protein concentration (hence Π_g) and bulk ISF protein concentration (hence Π_i); the 'race' between upstream diffusion and downstream washout, particularly at the junctional breaks, can result in a subglycocalyx protein concentration that is ~10% of C_i (*Figure 4A*). Under these circumstances, Π_g is so low that the effective osmotic pressure difference opposing fluid filtration approximates to Π_p rather than the classical Starling term $\Pi_p - \Pi_i$ (*Figure 2B*). This reduces basal J_v to similar levels as reported lymph drainage rates, and thus helps explain the low filtration force paradox.

7.2.3 Experimental tests of two-dimensional glycocalyx–cleft model

The Weinbaum model predicts that changes in Π_i around a filtering capillary should have much less effect on J_v than predicted by the classic Starling principle [Eq. (1c)]. The conflicting predictions were tested by Curry, Adamson and coworkers[60,83] with dramatic results (*Figure 4B*). When interstitial albumin concentration around rapidly filtering frog mesenteric capillaries was raised by superfusion to equal that perfused through the capillary lumen ($\Pi_p - \Pi_i = 0$), there was almost no change in the filtration rate—a finding incompatible with the classic Starling principle but in line with the Weinbaum model.[83] In a definitive study on rat mesenteric venules,[60] the increase in J_v caused by raising Π_i from zero to plasma level was ~20% of that predicted by the classic Starling principle. Measurements of filtration across confluent cultured endothelium in a Ussing-style chamber have likewise supported the glycocalyx–cleft model.[22]

7.2.4 Simplified one-dimensional model, time constants, and aquaporins

To facilitate computation and examine events during microvascular fluid uptake, Weinbaum and coworkers[84] developed a simplified

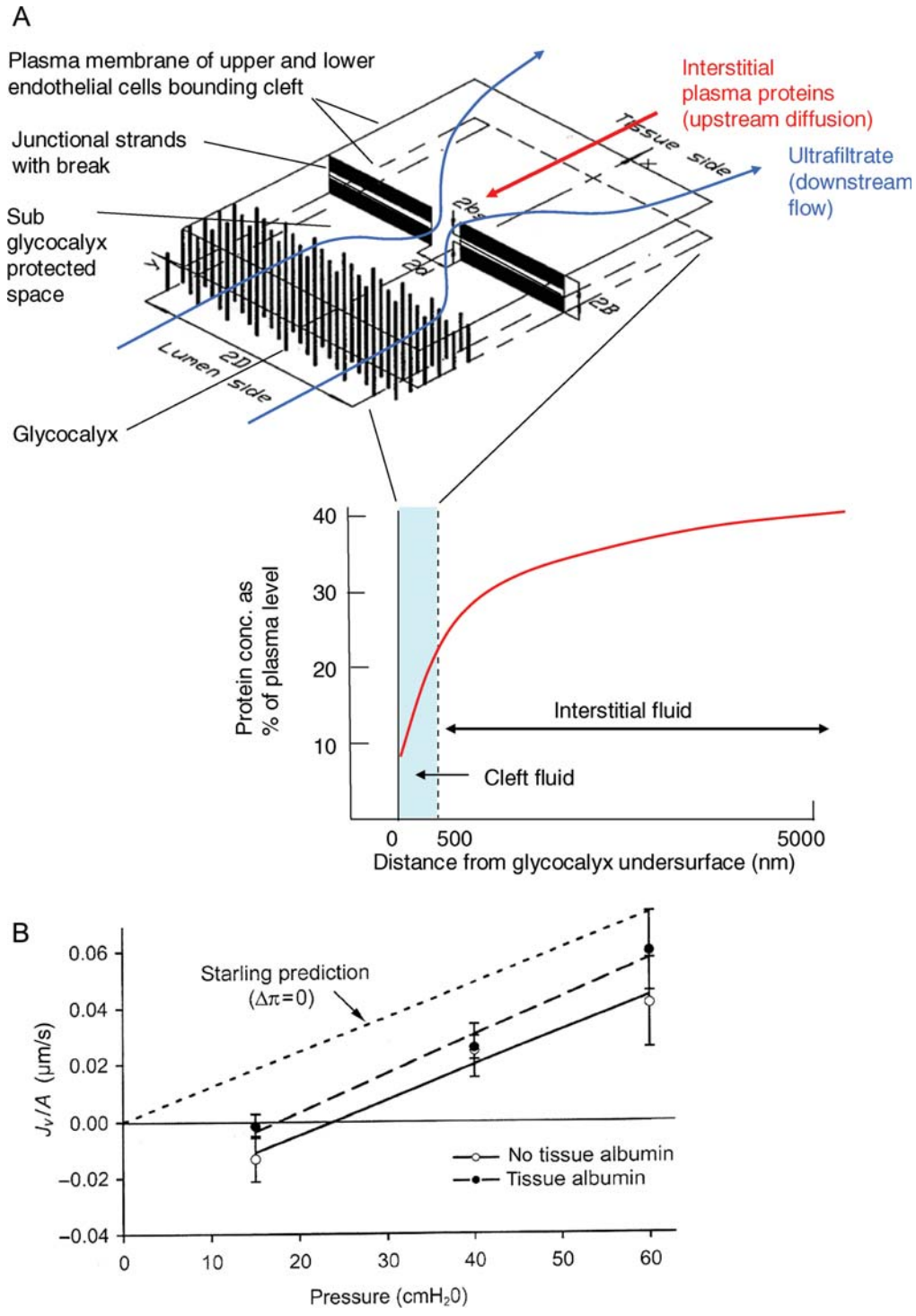

Figure 4 The two-dimensional glycocalyx–cleft model of capillary fluid exchange, and an experimental test of its predictions. (*A*) A mathematical model of the glycocalyx and intercellular cleft (top left).[82] The semipermeable glycocalyx layer is modelled as a set of fine rods. Graph shows calculated gradient of plasma protein from interstitium to the 'protected' subglycocalyx space, in a continuous capillary when $P_c > \Pi_p$. The subglycocalyx space is protected from equilibration with the bulk ISF by the convergent stream of ultrafiltrate passing through the narrow orifice formed by breaks in the intercellular junctional strands. (*B*) Fluid exchange in single rat mesenteric venules at controlled microvascular pressure, measured by the modified Landis red cell method (transient state).[60] The lumen was perfused with albumin solution and the exterior was superfused with saline ('no tissue albumin', open symbols; $\Pi_p - \Pi_i = \Pi_p$) or the same albumin solution as in the lumen ('tissue albumin', filled symbols; $\Pi_p - \Pi_i = 0$). Short dashes show the expected increase in filtration rate for the latter according to the classic Starling principle. The much smaller observed response was as predicted by the glycocalyx–cleft model. Steady-state results (data not shown) approximated to Eq. (3).

one-dimensional model, arguing that this more readily handles the differences in scale between the gradients inside the intercellular cleft and in the surrounding tissues. The one-dimensional model has been used to examine the transition from non-steady-state absorption to a low level of filtration. Zhang *et al.*[21] have argued that cuffs of pericytes encircling microvessels accelerate the transition from transient to steady-state fluid exchange by forming 'trapped microdomains' of fluid outside the vessels. They suggest that this phenomenon accounts for the rapid development of the steady state reported by Michel and Phillips[20] and confirmed in their own laboratory.[21] It is possible that trapped microdomains are not restricted to spaces beneath pericytes. Different tissues have different cellular architectures surrounding the microvessels, and this could contribute to the wide differences in the time constants of transition from transient to steady state.

The time constants could also be lengthened considerably if the aquaporin pathway contributes substantially to the microvascular L_p. Although Michel and Curry[56] concluded that aquaporins represent $\leq$10% of the L_p of most microvessels, Watson and Wolf[30–32] have argued that their contribution to L_p may be 40–50% in cat skeletal muscle capillaries. The osmotic pressures driving water through the aquaporin pathway are those of the capillary plasma and mean ISF. If aquaporins were responsible for 50% of L_p, once fluid absorption has started following a fall in P_c, it should continue until the reduction in ISF volume has concentrated the ISF proteins sufficiently for the consequent rise in Π_i to reduce $\Delta\Pi$ below ΔP. This could take an hour or more, as calculated using typical values for capillary L_p and ISF volume in skeletal muscle. Before regarding this as an explanation of the slow development of steady-state fluid exchange in skeletal muscle, a second consequence of a large aquaporin component of L_p should be considered. Since the osmotic pressure difference across the aquaporin pathway is Π_p minus the mean ISF Π_i (not Π_g), relatively high rates of fluid filtration should occur when P_c lies within its usual range (*Figure 2A*, right panel). One would therefore expect a brisk production of lymph in resting skeletal muscle—whereas resting lymph flow in skeletal muscle is so low that it is usually necessary to massage or passively exercise the muscle to obtain samples. Further investigation of the contribution of aquaporins and vasomotion to fluid exchange in skeletal muscle is required to resolve this question.

8. Clinical importance: increased endothelial permeability and tissue swelling

Microvascular fluid exchange underlies several major pathophysiological states. Starling himself was familiar with the transient absorption of ISF and attendant haemodilution following an acute hypotensive episode. Around 0.5 L of ISF can be absorbed into the human circulation within 15–30 min, supporting the cardiac output during hypotensive stress. Conversely, excessive microvascular filtration leads to interstitial oedema—a potentially fatal condition when it affects the lungs. Oedema can result from abnormal Starling's forces, increased endothelial permeability (e.g. inflammation), or impaired lymphatic drainage.[50] The biochemical processes mediating increases in endothelial permeability were reviewed recently by Mehta and Malik.[85] Here, we consider the impact of relatively small changes in endothelial membrane properties on fluid exchange.

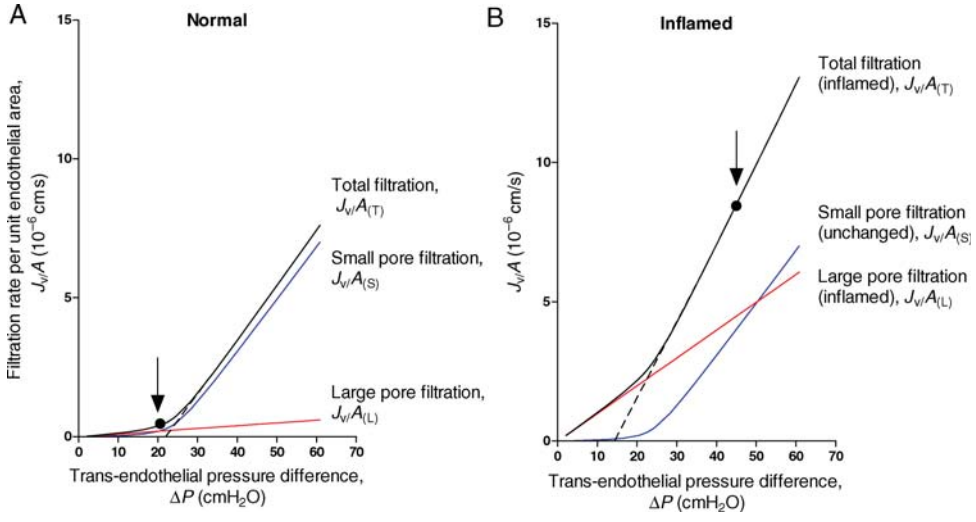

Figure 5 Steady-state fluid exchange simulated for a post-capillary venule, with the fluid-conducting pathways modelled as parallel small pore and large pore populations; effect of inflammation. (*A*) Basal low permeability state; 95% of the hydraulic conductance is represented by the small pores (radius = 4 nm; blue curve) and 5% by large pores (radius = 22.5 nm; red curve). The black solid curve shows the total fluid exchange (sum of red and blue lines) at varying values of P_c (see Appendix, end of this article). The vessel is perfused with a Ringer solution containing serum albumin (Π_p = 25 cmH_2O). P_i is assumed to be constant and aquaporin pathway negligible ($\leq$10% of total conductance). B. Steady-state fluid exchange when permeability has been increased in the same vessel. The red curve represents flow through the large pore system after inflammation has increased the number of large pores 10-fold. The small pore population is unchanged. The dashed lines are extrapolations of the linear parts of the steady-state summed relations to the pressure axis, where their intersection gives the value of the effective COP opposing fluid filtration (reduced in inflammation). Vertical arrows show typical values of microvascular pressure under basal conditions (*A*) and in mild inflammation (*B*). The rise in pressure contributes importantly to the dramatic 17-fold increase in filtration rate.

Substantial pathology can result from relatively small reductions in vascular barrier properties. Rippe and Haraldsson[86] pointed out that Eq. (3) describes fluid exchange through a homoporous membrane (one where all the fluid-conducting channels have the same hydraulic resistance and molecular-sieving properties); whereas endothelium has at least two fluid-conducting pathways, the 'small pore' and the 'large pore' pathways, as well as an aquaporin pathway in continuous capillaries. In normal healthy vessels, the small pores are estimated to contribute at least 95% and the large pores no more than 5% to the L_p of capillaries in skeletal muscle.[63,87] Using these values and Eq. (3), we have constructed curves for steady-state fluid exchange (*Figure 5A*); see Appendix. For models that also incorporate the low-conductance aquaporin pathway, see Wolf[31] and Rippe *et al.*[88] We have assumed that the small pore radius is 4 nm and the large pore radius is 22.5 nm. Since the large pores contribute only 5% to the L_P, this is equivalent to 19000 small pores for every large pore. In *Figure 5A*, we have plotted the separate relations between J_v/A and ΔP for the small and large pore systems, and the summated effect. Increased permeability can be thought of most simply as an increase in the number of large pores. *Figure 5B* shows the effect of a 10-fold increase in the number of large pores, with no change in the small pore population. The resulting increase in permeability resembles that seen during mild inflammation.[89] The increase in overall L_P is just over 50% and the overall σ to serum albumin falls only from 0.93 to 0.66. If the mean microvascular pressure were unchanged at just above 20 cmH_2O, the addition of nine large pores per 19 000 small pores would increase the fluid filtration rate five times. There would also be a noticeable increase in ISF protein concentration. The effect of this increase on J_v is greatly magnified by a rise in P_c, which results from the increased blood flow and vasodilatation of inflammation. If P_c rose to 40 cmH_2O (a relative modest increase), the net filtration of fluid into the tissue would increase 17-fold (arrow, *Figure 5B*). Very much larger increases in L_P and reductions in σ occur during the first phase of acute inflammation.[90–92] Changes of this magnitude are usually short-lived, however.

9. Advances in interstitial and lymphatic physiology

Space confines us to merely sketching advances in understanding the regulation of P_i and lymphatics. During acute inflammation P_i may fall initially, independently of microvascular exchange, and so amplify the initial rate of local oedema formation.[93] It is suggested that connective tissues are held under mild compression by collagen fibrils that are β_1-integrin bonded to fibroblasts and oppose the inherent tendency of interstitium to expand (glycosaminoglycan swelling). Fibril detachment serves to reduce P_i to more subatmospheric values. Supporting evidence includes a fall in P_i following treatment of the tissues with β_1-integrin antibodies.

The active role of lymphatics in clearing fluid away from peripheral tissues has been supported by investigations ranging from ion channel electrophysiology to human arm studies,[94,95] and lymphatic pump failure has been demonstrated in human breast cancer-related lymphoedema.[96] Advances in understanding the molecular and genetic control of lymphangiogenesis have underpinned insights into the defects that underlie some hereditary lymphoedemas.[97,98]

10. Summary and future directions

The COPs influencing filtration across both fenestrated and continuous capillaries are exerted across the endothelial glycocalyx; the osmotic pressure of the ISF does not directly determine transendothelial fluid exchange. There is substantial evidence that with important exceptions such as the renal cortex and medulla, downstream microvessels are not in a state of sustained fluid absorption as traditionally depicted. Although doggedly persistent in textbooks and teaching, the traditional view of filtration–reabsorption balance has little justification in the microcirculation of most tissues. Tissue fluid balance thus depends critically on lymphatic function in most tissues. In making these forceful statements, we are mindful of William Harvey's remark in his classic, *De Motu Cordis* (1628): 'I tremble lest I have mankind for my enemies, so much has wont and custom become second nature. Doctrine once sown strikes deep its root, and respect for antiquity influences all men'.[99]

We would emphasize that despite the above advances, much remain unknown. The time course of fluid absorption into the circulation requires more detailed investigation in a wider range of tissues; and the corresponding microstructure of the transendothelial pathway needs to be better defined, including estimates of the aquaporin contribution to the overall microvascular L_P, which appears to vary considerably.[32] The structure and composition of the glycocalyx over fenestrations and intercellular clefts should be explored. Understanding the regulation of the glycocalyx synthesis and turnover could lead to novel therapeutic strategies to reduce pathologically increased permeability. It also worth emphasizing that little is known of the nature of fenestral diaphragms; and that the classical problem of the transport of macromolecules through endothelia (large pores or vesicles) remains unresolved 50 years after it first became a controversy. Genetic knock-out mice offer a promising approach to some of these problems.[79,98]

Acknowledgements

We apologize to the many authors who have contributed importantly to this field and whose work has not been cited due to space limitations.

Conflict of interest: none declared.

References

1. Adair TH, Guyton AC. Modification of lymph by lymph nodes. II. Effect of increased lymph node venous blood pressure. *Am J Physiol* 1983;**245**:H616–H622.
2. Knox P, Pflug JJ. The effect of the canine popliteal node on the composition of lymph. *J Physiol* 1983;**345**:1–14.
3. Renkin EM. Some consequences of capillary permeability to macromolecules; Starling's hypothesis reconsidered. *Am J Physiol* 1986;**250**:H706–H710.
4. Starling EH. On the absorption of fluids from the connective tissue spaces. *J Physiol* 1896;**19**:312–326.
5. Staverman AJ. The theory of measurement of osmotic pressure. *Rec Trav Chim* 1951; **70**:344–352.
6. Kedem O, Katchalsky A. Thermodynamic analysis of the permeability of biological membranes to non-electrolytes. *Biochim Biophys Acta* 1958;**27**:229–245.
7. Landis EM. Micro-injection studies of capillary permeability. II. The relation between capillary pressure and the rate at which fluid passes through the walls of single capillaries. *Am J Physiol* 1927;**82**:217–238.
8. Pappenheimer JR, Soto-Rivera A. Effective osmotic pressure of the plasma proteins and other quantities associated with the capillary circulation in the hind-limbs of cats and dogs. *Am J Physiol* 1948;**152**:471–491.
9. Landis EM. Micro-injection studies of capillary blood pressure in human skin. *Heart* 1930;**30**:209–228.
10. Levick JR, Michel CC. The effects of position and skin temperature on the capillary pressures in the fingers and toes. *J Physiol* 1978;**274**:97–109.

11. Williams SA, Wasserman S, Rawlinson DW, Kitney RI, Smaje LH, Tooke JE. Dynamic measurement of human capillary blood pressure. *Clin Sci* 1988;**74**:507–512.
12. Starling EH. The production and absorption of lymph. In: Schäfer EA, ed. *Textbook of Physiology*. Vol. 1. Young J Pentland: Edinburgh; 1898. p285–p311.
13. Landis EM, Pappenheimer JR. Exchange of substances through the capillary walls. In: Hamilton WF, Dow P, eds. *Handbook of Physiology, Section 2: Circulation II*. Washington, DC: American Physiological Society; 1963. p961–1034.
14. Guyton AC, Granger HJ, Taylor AE. Interstitial fluid pressure. *Physiol Rev* 1971;**51**: 527–563.
15. Levick JR. *An Introduction to Cardiovascular Physiology*. 5th ed (Chapters 9, 10, 11). London: Hodder-Arnold; 2010.
16. Zweifach BW, Intaglietta M. Mechanics of fluid movement across single capillaries in the rabbit. *Microvasc Res* 1968;**1**:83–101.
17. Mahy IR, Tooke JR, Shore AC. Capillary pressure during and after incremental venous elevation in man. *J Physiol* 1995;**485**:213–219.
18. Bates DO, Levick JR, Mortimer PS. Starling pressure imbalance in the human arm and alteration in postmastectomy oedema. *J Physiol* 1994;**477**:355–363.
19. Levick JR. Capillary filtration-absorption balance reconsidered in light of dynamic extravascular factors. *Exp Physiol* 1991;**76**:825–857.
20. Michel CC, Phillips ME. Steady-state fluid filtration at different capillary pressures in perfused frog mesenteric capillaries. *J Physiol* 1987;**388**:421–435.
21. Zhang X, Adamson RH, Curry FE, Weinbaum S. Transient regulation of transport by pericytes in venular microvessels via trapped microdomains. *Proc Natl Acad Sci USA* 2008;**105**:1374–1379.
22. Pang Z, Tarbell JM. In vitro study of Starling's hypothesis in a cultured monolayer of bovine aortic endothelial cells. *J Vasc Res* 2003;**40**:351–358.
23. Taylor AE, Granger DN. Exchange of macromolecules across the microcirculation. In: Renkin EM, Michel CC, eds. *Handbook of Physiology, Section 2: The Cardiovascular System, Vol. IV: The Microcirculation*. American Physiological Society; 1984. p467–520.
24. Renkin EM, Joyner WL, Sloop CH, Watson PD. Influence of venous pressure on plasma-lymph transport in the dog's paw: convective and dissipative mechanisms. *Microvasc Res* 1977;**14**:191–204.
25. Cohnheim J. *Lectures on General Pathology. Vol. 1: The Circulation*. New Sydenham Edition; 1889. p515.
26. Taylor AE, Townsley MI. Evaluation of the Starling fluid flux equation. *News Physiol Sci* 1987;**2**:48–52.
27. Michel CC. Fluid movement through capillary walls. In: Renkin EM, Michel CC, eds. *Handbook of Physiology, Section 2: The Cardiovascular System, Vol. IV: The Microcirculation*. Bethesda: American Physiological Society; 1984. p375–409.
28. Guyton AC, Lindsey AW. Effect of elevated left atrial pressure and decreased plasma protein concentration on the development of pulmonary oedema. *Circ Res* 1959;**7**: 649–657.
29. Landis EM Gibbon JH. The effect of temperature and tissue pressure on the movement of fluid through the human capillary wall. *J Clin Invest* 1933;**12**:105–138.
30. Wolf MB, Watson PD. Measurement of the osmotic reflection coefficient for small molecules in cat hindlimb. *Am J Physiol* 1989;**256**:H282–H290.
31. Wolf MB. Determination of the magnitude of the water-exclusive pathway in cat skeletal muscle microvasculature. *Microcirculation* 1996;**3**:59–73.
32. Wolf MB. A three-pathway pore model describes extensive data from mammalian microvascular beds and frog microvessels. *Microcirculation* 2002;**6**:497–511.
33. Gore RW, Bohlen HG. Microvascular pressures in rat intestinal muscle and mucosal villi. *Am J Physiol* 1978;**233**:H685–H693.
34. Granger DN, Taylor AE. Effects of solute-coupled transport on lymph flow and oncotic pressure in cat ileum. *Am J Physiol* 1978;**235**:E429–E436.
35. Granger DN, Mortillaro NA, Kvietys PR, Rutili G, Taylor AE. Role of the interstitial matrix during intestinal volume absorption. *Am J Physiol* 1980;**238**:G183–G189.
36. Pappenheimer JR, Michel CC. Role of villus microcirculation in intestinal absorption of glucose; coupling of epithelial with endothelial transport. *J Physiol* 2003;**553**: 561–574.
37. Ulfendahl HR, Wolgast M. Renal circulation and lymphatics. In: Seldin DW, Giebisch G, eds. *The Kidney: Physiology and Pathophysiology*. New York: Raven Press Ltd; 1992. p1017–1047.
38. Lassen NA, Longley JB, Lilienfield L. Concentration of albumin in renal papilla. *Science* 1958;**128**:720–721.
39. Williams MMM, Moffat DB, Creasy M. The effect of antidiuretic hormone on the permeability of the vessels of the renal medulla of the rat during water diuresis. *Q J Exp Physiol* 1971;**56**:250–256.
40. Venkatachalam MA, Karnovsky MJ. Extravascular protein in the kidney: an ultrastrucutural study of its relation to renal peritubular capillary permeability using protein tracers. *Lab Invest* 1972;**27**:435–444.
41. Schmidt-Nielsen B. The renal pelvis. *Kidney Int* 1987;**31**:621–628.
42. Tenstad O, Heyeraas KJ, Wiig H, Aukland K. Drainage of plasma proteins from the renal medullary interstitium in rats. *J Physiol* 2001;**536**:533–539.
43. MacPhee PJ, Michel CC. Fluid uptake from the renal medulla into the ascending vasa recta in anaesthetized rats. *J Physiol* 1995b;**487**:169–183.
44. Pallone TL. Molecular sieving of albumin by the ascending vasa recta wall. *J Clin Invest* 1992;**90**:30–34.
45. Michel CC. Renal medullary microcirculation: architecture and exchange. *Microcirculation* 1995;**2**:125–139.
46. Wang W, Michel CC. Modeling the exchange of plasma protein between the microcirculation and the interstitium of the renal medulla. *Am J Physiol Renal Physiol* 2000; **279**:F333–F344.
47. Zhang W, Edwards A. Transport of plasma proteins across the vasa recta in the renal medulla. *Am J Physiol Renal Physiol* 2001;**281**:F478–F492.
48. MacPhee PJ, Michel CC. Sub-atmospheric closing pressures in individual microvessels in rats and frogs. *J Physiol* 1995a;**484**:183–187.
49. Takahashi-Iwanaga H. Three dimensional cytoarchitecture of the interstitial tissue in the rat kidney. *Cell Tissue Res* 1991;**264**:269–281.
50. Mortimer PS, Levick JR. Chronic peripheral oedema: the critical role of the lymphatic system. *Clin Med* 2004;**4**:448–453.
51. Aukland K, Reed RK. Interstitial-lymphatic mechanisms in the control of extracellular fluid volume. *Physiol Rev* 1993;**73**:1–78.
52. Chambers R, Zweifach BW. Intercellular cement and capillary permeability. *Physiol Rev* 1947;**27**:436–463.
53. Intaglietta M, Endrich B. Experimental and quantitative analysis of microcirculatory water exchange. *Acta Physiol Scand Suppl* 1979;**463**:59–66.
54. McDonald JN, Levick JR. Effect of extravascular plasma protein on pressure-flow relations across synovium in anaesthetized rabbits. *J Physiol* 1993;**465**:539–559.
55. Levick JR. An analysis of the interaction between extravascular plasma protein, interstitial flow and capillary filtration; application to synovium. *Microvasc Res* 1994;**47**: 90–125.
56. Michel CC, Curry FE. Microvascular permeability. *Physiol Rev* 1999;**79**:703–761.
57. Pallone TL, Kishore BK, Nielsen S, Agre P, Knepper M. Evidence that aquaporin-1 mediates NaCl induced water flux across descending vasa recta. *Am J Physiol* 1997;**272**:F587–F596.
58. Wissig SL, Williams MC. The permeability of muscle capillaries to microperoxidase. *J Cell Biol* 1978;**76**:341–359.
59. Adamson RH, Michel CC. Pathways through the intercellular clefts of frog mesenteric capillaries. *J Physiol* 1993;**466**:303–327.
60. Adamson RH, Lenz JF, Zhang X, Adamson GN, Weinbaum S, Curry FE. Oncotic pressures opposing filtration across non-fenestrated rat microvessels. *J Physiol* 2004;**557**:889–908.
61. Pappenheimer JR, Renkin EM, Borrero LM. Filtration, diffusion and molecular sieving through peripheral capillary membranes. A contribution to the pore theory of capillary permeability. *Am J Physiol* 1951;**167**:13–46.
62. Renkin EM. Multiple pathways of capillary permeability. *Circ Res* 1977;**41**:735–743.
63. Rippe B, Haraldsson B. Transport of macromolecules across microvascular walls: the two-pore theory. *Physiol Rev* 1994;**74**:163–219.
64. Curry FE, Michel CC. A fibre-matrix model of capillary permeability. *Microvasc Res* 1980;**20**:96–99.
65. Rostgaard J, Qvortrup K. Electron microscopic demonstrations of filamentous molecular sieve plugs in capillary fenestrae. *Microvasc Res* 1997;**53**:1–13.
66. Squire JM, Chew M, Nnedji G, Neal C, Barry J, Michel CC. Quasi-periodic substructure in the microvessel endothelial glycocalyx: a possible explanation for molecular filtering? *J Struct Biol* 2001;**136**:239–255.
67. Reitsma S, Slaaf DW, Vink H, van Zandvoort, oude Egbrink MG. The endothelial glycocalyx: composition, functions and visualization. *Pflügers Arch* 2007;**254**:345–359.
68. Weinbaum S, Tarbell JM, Damiano ER. The structure and function of the endothelial glycocalyx layer. *Ann Rev Biomed Eng* 2007;**9**:121–167.
69. Levick JR, Michel CC. The effect of bovine serum albumin on the permeability of frog mesenteric capillaries. *Quart J Exp Physiol* 1973;**58**:87–97.
70. Turner MR, Clough G, Michel CC. The effects of cationized ferritin and native ferritin upon the filtration coefficient of single frog capillaries. Evidence that proteins in the endothelial cell coat influence permeability. *Microvasc Res* 1983;**25**:205–222.
71. Schneeberger EE, Hamelin M. Interaction of serum proteins with lung endothelial glycocalyx: its effect on endothelial permeability. *Am J Physiol* 1984;**247**:H206–H217.
72. Powers MR, Blumenstock FA, Cooper JA, Malik AB. Role of albumin arginyl sites in albumin-induced reduction of endothelial hydraulic conductivity. *J Cell Physiol* 1989; **141**:558–564.
73. Adamson RH. Permeability of frog mesenteric capillaries after partial pronase digestion of the endothelial glycocalyx. *J Physiol* 1990;**428**:1–13.
74. Henry CBC, Duling BR. Permeation of the luminal capillary glycocalyx is determined by hyaluronan. *Am J Physiol* 1999;**277**:H508–H514.
75. Vink H, Duling BR. Identification of distinct luminal domains for macromolecules, erythrocytes and leukocytes within mammalian capillaries. *Circ Res* 1996;**79**: 581–589.
76. Lopez-Quintero SV, Amaya R, Pahakis M, Tarbell JM. The endothelial glycocalyx mediates shear-induced changes in hydraulic conductivity. *Am J Physiol* 2009;**296**: H1451–H1456.
77. Bruns RR, Palade GE. Studies on blood capillaries. II. Transport of ferritin molecules across the wall of muscle capillaries. *J Cell Biol* 1968;**37**:277–299.
78. Clough G, Michel CC. The role of vesicles in the transport of ferritin through frog endothelium. *J Physiol* 1981;**315**:127–142.

79. Rosengren B-I, Rippe A, Rippe C, Venturoli D, Sward K, Rippe B. Transvascular protein transport in mice lacking endothelial caveolae. *Am J Physiol* 2006;**291**: H1371–H1377.
80. Michel CC. Starling: The formulation of his hypothesis of microvascular fluid exchange its significance after 100 years. *Exp Physiol* 1997;**82**:1–30.
81. Weinbaum S. 1997 Whittaker distinguished lecture: Models to solve mysteries in biomechanics at a cellular level; a new view of fibre matrix layers. *Ann Biomed Eng* 1998;**26**:1–17.
82. Hu X, Weinbaum S. A new view of Starling's hypothesis at the microstructural level. *Microvasc Res* 1999;**58**:281–304.
83. Hu X, Adamson RH, Liu B, Curry FE, Weinbaum S. Starling forces that oppose filtration after tissue oncotic pressure is increased. *Am J Physiol* 2000;**279**: H1724–H1736.
84. Zhang X, Adamson RH, Curry FE, Weinbaum S. A 1-D model to explore the effects of tissue loading and tissue concentration gradients in the revised Starling principle. *Am J Physiol* 2007;**291**:H2950–H2964.
85. Mehta D, Malik AB. Signaling mechanisms regulating endothelial permeability. *Physiol Rev* 2006;**86**:279–367.
86. Rippe B, Haraldsson B. On the steady-state relationship between the microvascular hydrostatic pressure and the transvascular filtration rate. Effects of heteroporosity. *Acta Physiol Scand* 1987;**129**:441–442.
87. Rippe B, Haraldsson B. Fluid and protein fluxes across the microvasculature. Application of two-pore equations. *Acta Physiol Scand* 1987;**131**:411–428.
88. Rippe B, Rosengren B-I, Venturoli D. The peritoneal microcirculation in peritoneal dialysis. *Microcirculation* 2001;**8**:303–320.
89. Michel CC, Kendall S. Differing effects of histamine and serotonin on microvascular permeability in anaesthetized rats. *J Physiol* 1997;**501**:657–662.
90. Bates DO, Curry FE. Vascular endothelial growth factor increases hydraulic conductivity of isolate perfused microvessels. *Am J Physiol* 1996;**271**:H2520–H2528.
91. Adamson RH, Zeng M, Adamson GN, Lenz JF, Curry FE. PAF- and bradykinin-induced hyperpermeability of rat venules is independent of actin-myosin contraction. *Am J Physiol* 2003;**285**:H406–H417.
92. Pocock TM, Foster RR, Bates DO. Evidence of a role for TRPC channels in VEGF mediated increased microvascular permeability *in vivo*. *Am J Physiol* 2004;**286**: H1015–H1026.
93. Wiig H, Rubin K, Reed RK. New and active role of the interstitium in control of interstitial fluid pressure: potential therapeutic consequences. *Acta Anaesth Scand* 2003;**47**:111–121.
94. Levick JR, McHale N. Physiology of lymph production and propulsion. In: Browse N, Burnand K, Mortimer PS, eds. *Diseases of the Lymphatics*. London: Edward Arnold; 2003. p44–64.
95. Zawieja D. Lymphatic biology and the microcirculation: past, present and future. *Microcirculation* 2005;**12**:141–150.
96. Stanton AWB, Modi S, Mellor RH, Levick JR, Mortimer PS. Recent advances in breast cancer-related lymphoedema of the arm: lymphatic pump failure and predisposing factors. *Lymphatic Res Biol* 2009;**7**:29–45.
97. Alitalo K, Tammela T, Petrova T. Lymphangiogenesis in development and human disease. *Nature* 2005;**438**:946–953.
98. Karlsen TV, Karkkainen MJ, Alitalo K, Wiig H. Transcapillary fluid balance consequences of missing initial lymphatics studied in a mouse model of primary lymphoedema. *J Physiol* 2006;**574**:583–596.
99. Harvey W. *On the motion of the Heart and Blood in Animals* (trans. by R. Willis). Buffalo, New York: Prometheus Books; 1993.
100. Curry FE. Mechanics and thermodynamics of transcapillary exchange. In: Renkin EM, Michel CC, eds. *Handbook of Physiology, Section 2: The Cardiovascular Sysytem, Vol. 4: Microcirculation*. Chapter 8. Bethesda, MD: American Physiological Society; 1984. p309–374.

Appendix: two-pore model used to generate *Figure 5*

The method was that described by Rippe and Haraldssson,[63,87] where the capillary wall is modelled as an impermeable membrane of thickness Δx penetrated by two sets of cylindrical pores—small pores of radii 4 nm and large pores of radii 22.5 nm. L_p was chosen to be 2×10^{-7} cm s^{-1} H$_2$O^{-1} (typical of a rat mesenteric venule), 95% of which was accounted for by small pores and 5% by large pores. Thus, for the small pores $L_{p(S)} = 1.9 \times 10^{-7}$ cm s^{-1} cmH$_2$O^{-1} and for the large pores $L_{p(L)} = 0.1 \times 10^{-7}$ cm s^{-1} cmH$_2$O^{-1} and the overall hydraulic conductance is

$$L_p(\text{overall}) = L_{p(S)} + L_{p(L)} \tag{A1}$$

Pore theory (e.g. Curry[100]) defines the L_p of a population of pores of constant radius (r) in terms of Poiseuille's law, i.e.

$$L_p = \frac{\pi r^4 N}{\Delta x 8 \eta} \tag{A2}$$

where N is the number of pores per unit area of membrane and η is the fluid viscosity within the pores. Thus, by assigning values for $L_{p(S)}$ and $L_{p(L)}$ and pore radii, we have determined the values of $N_S/\Delta x$ and $N_L/\Delta x$, the ratios of the numbers of small and large pores to their length.

The partition coefficient, λ, and the reflection coefficient, σ, for each set of pores to a particular solute depend on the ratio of the molecular radius (a) to the pore radius. They have been calculated from the following expressions:

$$\lambda = \left(1 - \frac{a}{r}\right)^2 \tag{A3}$$

and

$$\sigma = (1 - \lambda)^2 \tag{A4}$$

Finally, the diffusional permeability, p, of the solute for each set of pores is related to the diffusion coefficient of the solute in aqueous solution, D, and a function dependent on (a/r):

$$p = \frac{\pi r^2 N}{\Delta x} \lambda D f\,(a/r) \tag{A5}$$

where

$$f\left(\frac{a}{r}\right) = 1 - 2.1\left(\frac{a}{r}\right) + 2.09\left(\frac{a}{r}\right)^3 - 0.95\left(\frac{a}{r}\right)^5 \cdots \tag{A6}$$

Equations (A1)–(A6) were used to estimate the values for L_p, σ and p for serum albumin at each population of pores, assuming that $a = 3.6$ nm for albumin. Equation (3) was re-arranged as

$$\Delta P = \frac{J_V/A}{L_p} + \sigma^2 \Pi_p \frac{(1 - e^{-Pe})}{(1 - \sigma \cdot e^{-Pe})} \tag{A7}$$

with the relevant values of L_p, σ, and p, equation (A7) was used to determine the values of ΔP for a range of values of J_V/A for the small pores and the large pores. The values of J_V/A at the same ΔP for the small pores and the large pores were added to give the overall J_V/A for unit area of vessel wall (*Figure 5A*). The exercise was repeated for *Figure 5B*. Here, the contribution of $L_{P(S)}$ remained constant at 1.9×10^{-7} cm s^{-1} H$_2$O^{-1} and $L_{p(L)}$ was increased 10-fold, raising the overall L_p only modestly, from 2.0 to $(1.9 + 1.0) = 2.9 \times 10^{-7}$ cm s^{-1} H$_2$O^{-1}.